Open and Hidden Charm Production in dA Collisions at RHIC and LHC

R. Vogt

Nuclear Science Division, Lawrence Berkeley National Laboratory, Berkeley, CA 94720, USA

Physics Department, University of California, Davis, CA 95616, USA

Charm is Hard Process, Calculable in Perturbative QCD

'Hard' processes have a large scale in the calculation that makes perturbative QCD applicable: high momentum transfer, μ^2, high mass, m, high transverse momentum, p_T

Asymptotic freedom assumed to calculate the interactions between two hadrons on the quark/gluon level but the confinement scale determines the probability of finding the interacting parton in the initial hadron

Factorization assumed between the perturbative hard part and the universal, nonperturbative parton distribution functions

The hadronic cross section in an AB collision where $AB = pp, pA$ or nucleus-nucleus is

$$\sigma_{AB}(S, m^2) = \sum_{i,j=q,\overline{q},g} \int_{4m_Q^2/s}^1 \frac{d\tau}{\tau} \int dx_1\, dx_2\, \delta(x_1 x_2 - \tau) \times f_i^A(x_1, \mu_F^2)\, f_j^B(x_2, \mu_F^2)\, \widehat{\sigma}_{ij}(s, m^2, \mu_F^2, \mu_R^2)$$

f_i^A are the nonperturbative parton distributions, determined from fits to data, x_1 and x_2 are the fractional momentum of hadrons A and B carried by partons i and j, $\tau = s/S$

$\widehat{\sigma}_{ij}(s, m^2, \mu_F^2, \mu_R^2)$ is hard partonic cross section calculable in QCD in powers of α_s^{2+n}: leading order (LO), $n = 0$; next-to-leading order (NLO), $n = 1$ ...

Results depend strongly on quark mass, m, factorization scale, μ_F, in the parton densities and renormalization scale, μ_R, in α_s

Fixing NLO Parameters m and μ^2 to All Data

Difficult to obtain a large calculated $c\overline{c}$ cross section with $\mu_F^2 = \mu_R^2$, as in parton density fits

Data favors lower masses – lowest mass used here is 1.2 GeV but much lower masses than allowed in pQCD needed to agree with largest cross sections

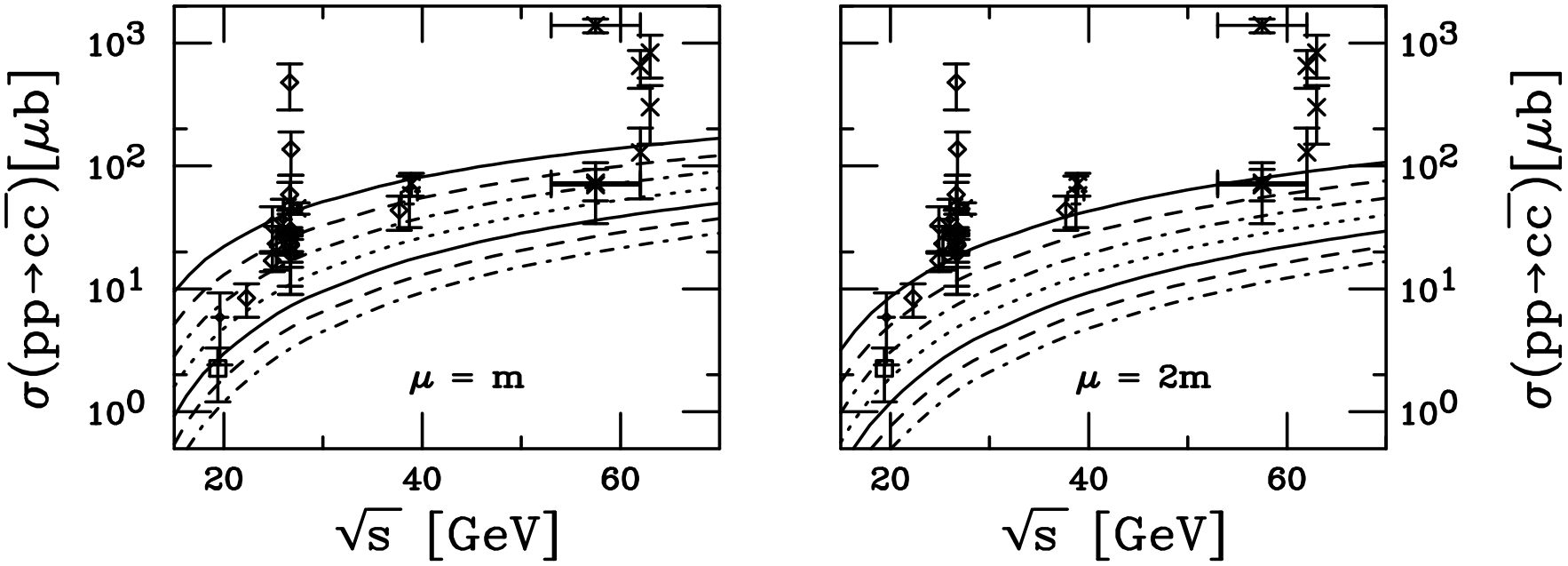

Figure 1: Total $c\overline{c}$ cross sections in pp and pA interactions up to ISR energies as a function of the charm quark mass. All calculations are fully NLO using the MRST HO (central gluon) parton densities. The left-hand plot shows the results with the renormalization and factorization scales equal to m while in the right-hand plot the scale is set to $2m$. From top to bottom the curves are $m = 1.2$, 1.3, 1.4, 1.5, 1.6, 1.7, and 1.8 GeV.

Extrapolation to Higher Energies

Only two curves remain, MRST HO with $m = 1.2$ GeV, $\mu^2 = 4m^2$ and GRV98 HO with $m = 1.3$ GeV, $\mu^2 = m^2$

We have kept only the most recent measurements, including the PHENIX $\sqrt{S} = 130$ GeV result from Au+Au, lowest $\sqrt{S} = 200$ GeV point is from PHENIX pp

The current STAR point lies well above these results

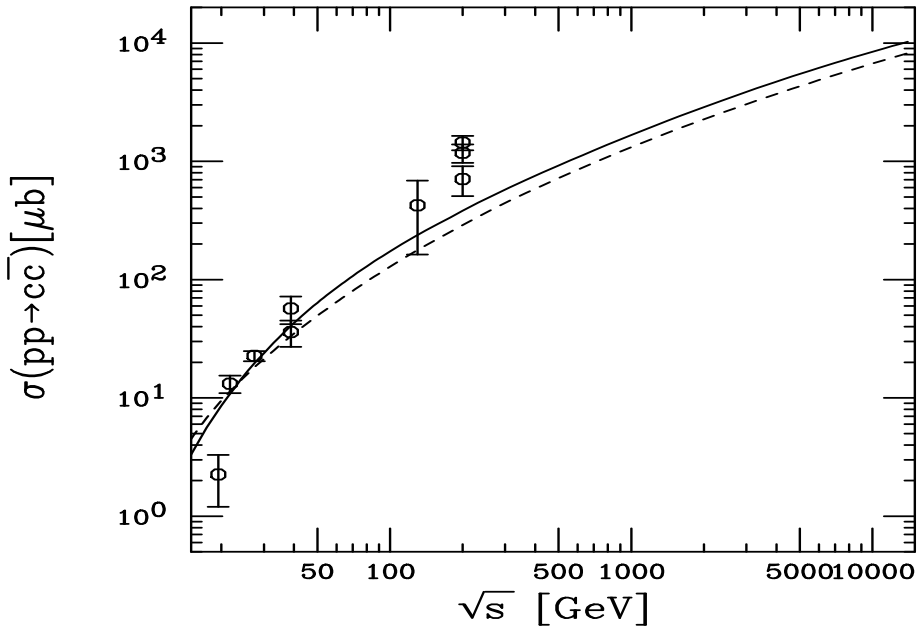

Figure 2: Total $c\bar{c}$ cross sections in pp interactions up to 14 TeV. All calculations are fully NLO. The curves are MRST HO (central gluon) with $m = 1.2$ GeV and $\mu^2 = 4m^2$ (dashed) and GRV98 HO with $m = 1.3$ GeV and $\mu^2 = m^2$.

From Total Cross Sections to Distributions

In total cross section, the quark mass is the only relevant scale

When considering kinematic observables like x_F or p_T, the momentum scale is also relevant so that, instead of $\mu^2 \propto m^2$, one usually uses $\mu^2 \propto m_T^2$

Other important considerations for distributions: fragmentation and intrinsic k_T

Fragmentation assumed to be universal, like parton densities, so the parameterizations of e^+e^- data (*e.g.* Peterson function) should work in hadroproduction

Effect of intrinsic transverse momentum broadening decreases with energy

Bare Quark p_T Distributions as a Function of m and μ

Differences largest at low p_T, determines total cross section

Distributions become similar at high p_T

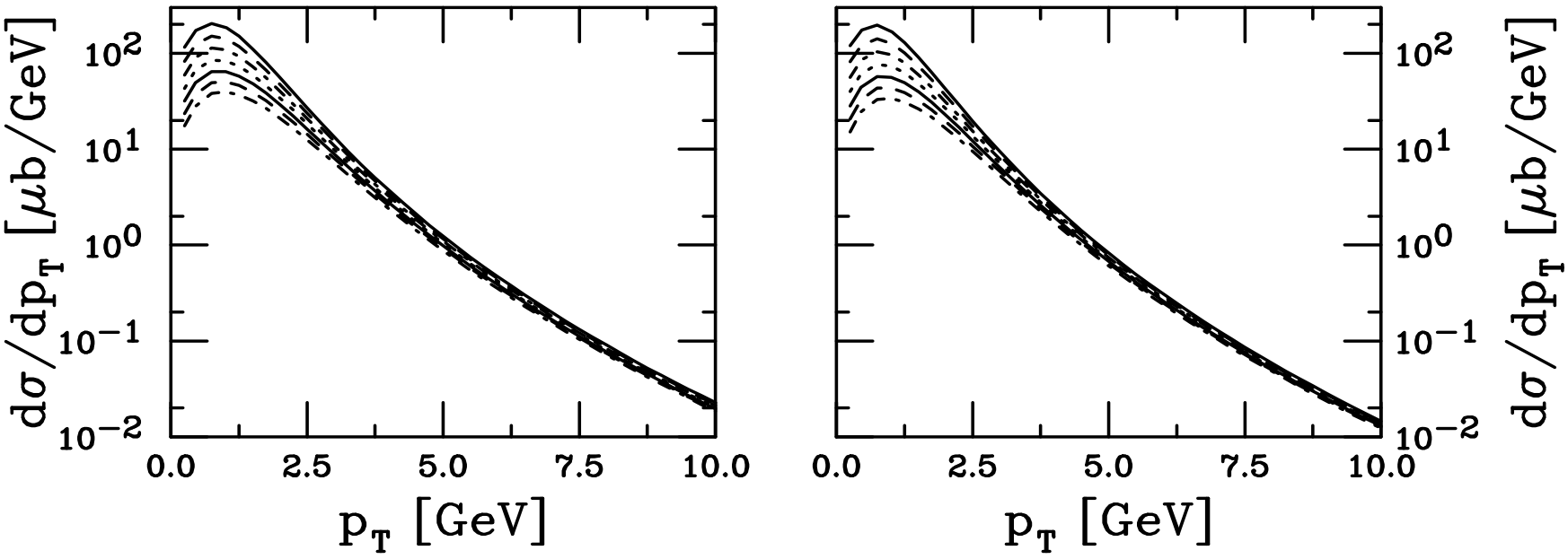

Figure 3: The NLO charm quark p_T distributions in pp interactions at $\sqrt{S} = 200$ GeV as a function of the charm quark mass calculated with the GRV98 HO parton densities, integrated over all rapidity. The left-hand plot shows the results with the renormalization and factorization scales equal to m_T while in the right-hand plot the scale is set to $2m_T$. From top to bottom the curves are $m = 1.2$, 1.3, 1.4, 1.5, 1.6, 1.7, and 1.8 GeV.

Average Bare Quark p_T as a Function of m and μ

Average p_T increases with m and decreases with μ

	$\mu = m_T$	$\mu = 2m_T$
m_c (GeV)	$\langle p_T \rangle$ (GeV)	$\langle p_T \rangle$ (GeV)
1.2	1.17	1.08
1.3	1.23	1.15
1.4	1.29	1.21
1.5	1.35	1.28
1.6	1.41	1.35
1.7	1.48	1.41
1.8	1.54	1.48

Table 1: Average charm quark p_T for various mass and scale combinations.

Parameter Variation of p_T Distributions

Ratios of cross sections relative to $m = 1.2$ GeV shows largest difference at low p_T, similar results for $\mu = m_T$ and $2m_T$

Ratio of cross sections with $\mu = 2m_T$ relative to those with $\mu = m_T$ at the same mass value are almost independent of mass

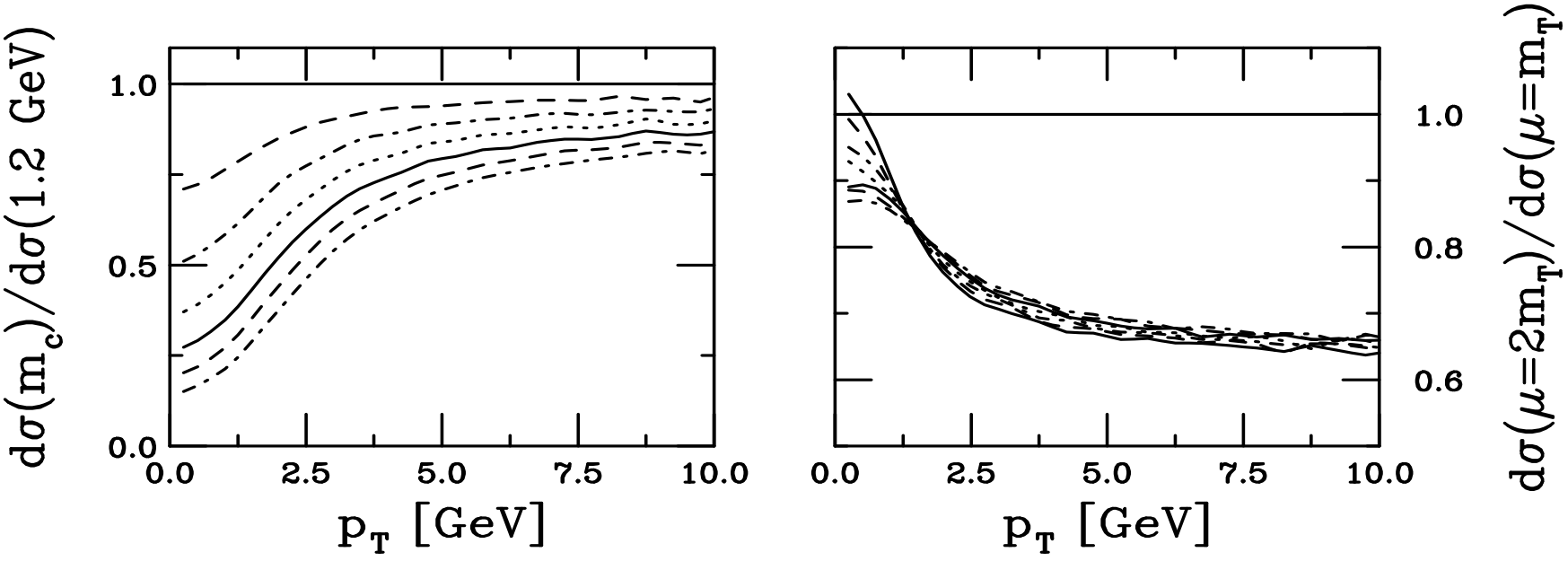

Figure 4: The ratios NLO charm quark p_T distributions in pp interactions at $\sqrt{S} = 200$ GeV as a function of the charm quark mass calculated with the GRV98 HO parton densities. The left-hand plot shows the ratio of the p_T distributions to that with $m = 1.2$ GeV while the right-hand plot shows the ratio of the result with $\mu = 2m_T$ relative to $\mu = m_T$ for each value of m. From top to bottom the curves are $m = 1.2$, 1.3, 1.4, 1.5, 1.6, 1.7, and 1.8 GeV.

Adding Fragmentation and Intrinsic k_T

Double differential cross sections

$$s^2 \frac{d^2\sigma_{pp}(s,t,u)}{dtdu} = \sum_{i,j=q,\overline{q},g} \int_{x_1^-}^1 \frac{dx_1}{x_1} \int_{x_2^-}^1 \frac{dx_2}{x_2} f_i^p(x_1,\mu^2) f_j^p(x_2,\mu^2) \mathcal{J}_K(\hat{s},\hat{t},\hat{u}) \hat{s}^2 \frac{d^2\hat{\sigma}_{ij}(\hat{s},\hat{t},\hat{u})}{d\hat{t}d\hat{u}}$$

$f_i^p = F_i^p/x$ is parton density, $\mathcal{J}_K$ is a kinematics-dependent Jacobian

Intrinsic transverse momentum and fragmentation are needed to smear the pair p_T and ϕ distributions as measured for $D\overline{D}$ correlations (Peterson fragmentation and $k_T^2 = 1$ GeV^2 cancel each other in low $\sqrt{S}$ single D p_T distributions)

Adds the following extra integrations:

$$\int dz_3 dz_4 d^2k_{T1} d^2k_{T2} \frac{D_{H/Q}(z_3,\mu^2)}{z_3} \frac{D_{\overline{H}/\overline{Q}}(z_4,\mu^2)}{z_4} g_p(k_{T1}) g_p(k_{T2})$$

Fragmentation function a la Peterson

$$D_{H/Q}(z) = \frac{N}{z(1-1/z-\epsilon_Q/(1-z))^2}$$

$\epsilon_Q = 0.06$ for charm, 0.006 for bottom, normalized so that $\Sigma_H \int D_{H/Q}(z)dz = 1$ for all H hadrons from Q

Gaussian k_T smearing, $\langle k_T^2 \rangle_p = 1$ GeV^2 for pp, broadened for pA and AA, NLO code adds in final state

$$g_p(k_T) = \frac{1}{\pi \langle k_T^2 \rangle_p} \exp(-k_T^2/\langle k_T^2 \rangle_p)$$

Bare Quark Distribution Works Better for x_F

$x_F = 2p_L/\sqrt{S} = 2m_T \sinh y/\sqrt{S}$ distributions integrated over p_T, average goes into m_T in x_F

$pp \to DX$ at 400 GeV, fixed target shown here

Bare distribution (delta function) works better than the Peterson function (dashed curve) which falls below data

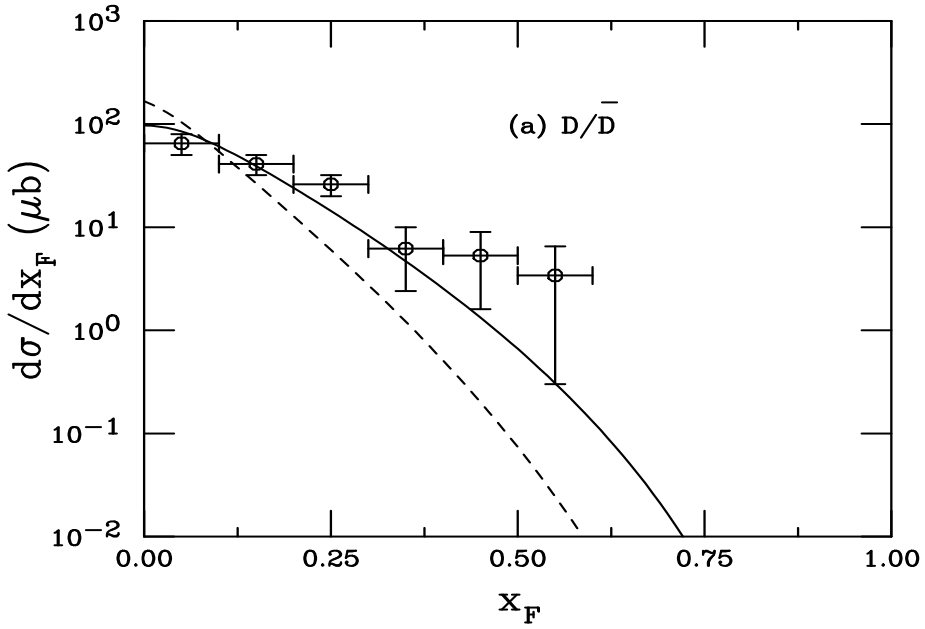

Figure 5: Comparison of calculations with data from 400 GeV pp interactions. The dashed curve uses the Peterson function while the solid curve is a delta function. The data are from M. Aguilar-Benitez *et al.*, Phys. Lett. **B189**, 476 (1987), the calculations from R.V. *et al.*, Nucl. Phys. **B383**, 643 (1992).

Cancellation of Fragmentation and k_T at $\sqrt{S} = 16$ GeV

Bare charm (solid) and Peterson fragmentation with $\langle k_T^2 \rangle = 1$ GeV^2 (dotted) on top of each other

Broadening alone, $\langle k_T^2 \rangle = 1$ GeV^2, widens p_T distribution

Peterson fragmentation alone (dot-dashed) below bare

Large $\langle k_T^2 \rangle$ (dot-dot-dot-dashed) in between

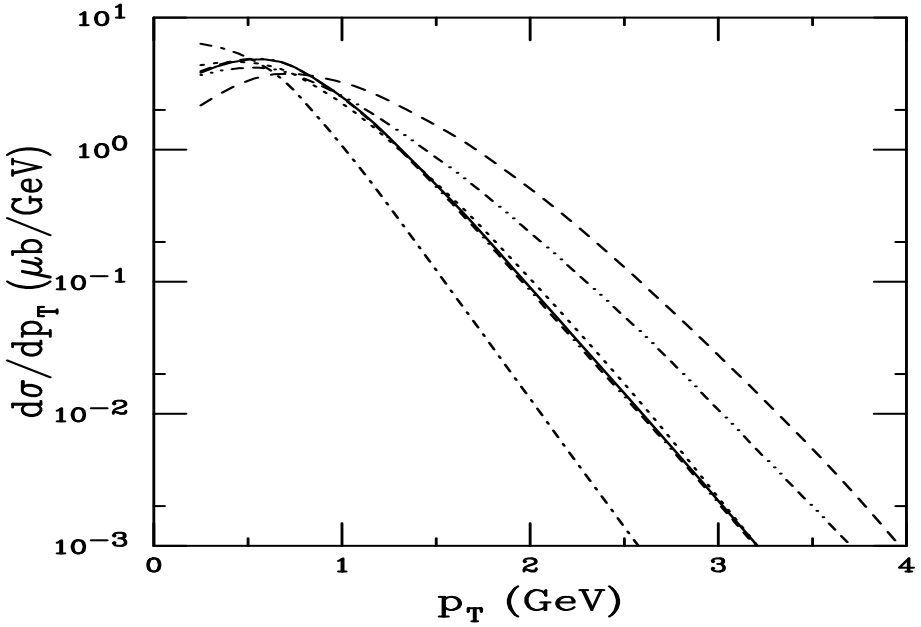

Figure 6: For a fixed-target experiment with $p_{\rm lab} = 158$ GeV, we compare the NLO p_T distributions including fragmentation and intrinsic k_T. The solid curves shows the bare distribution, the dashed includes $\langle k_T^2 \rangle = 1$ GeV^2 but no fragmentation, the dot-dashed is Peterson fragmentation alone, the dotted and dot-dot-dot-dashed include both Peterson fragmentation and broadening with $\langle k_T^2 \rangle = 1$ and 1.7 GeV^2 respectively.

No Cancellation at RHIC

$\langle k_T^2 \rangle = 1$ GeV^2 alone (dashed) is now a small effect since $\langle p_T \rangle$ is much larger than at fixed-target energies

Peterson fragmentation alone (dot-dashed) below bare distribution, going to higher $\langle k_T^2 \rangle$ does not help, 1.7 GeV^2 is largest shown, even 4 GeV^2 does not bring the result closer to the bare distribution

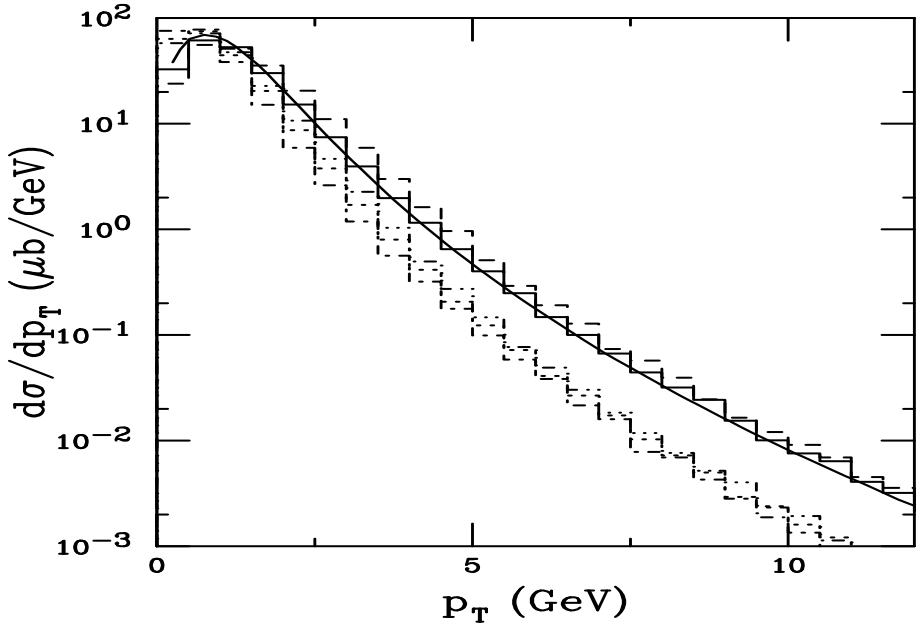

Figure 7: We compare the NLO p_T distributions including fragmentation and intrinsic k_T at $\sqrt{S_{NN}} = 200$ GeV. The solid curve and solid histogram shows the bare distribution calculated both as a single inclusive distribution and in exclusive pair production, the dashed includes $\langle k_T^2 \rangle = 1$ GeV^2 but no fragmentation, the dot-dashed is Peterson fragmentation alone, the dotted and dot-dot-dot-dashed include both Peterson fragmentation and broadening with $\langle k_T^2 \rangle = 1$ and 1.7 GeV^2 respectively.

Dependence of p_T Distributions on Parton Densities

Both MRST HO and GRV98 HO parton densities agree well with lower energy data for total cross section

Preliminary STAR reconstructed D and D^* data agree with shape of NLO bare quark p_T distribution

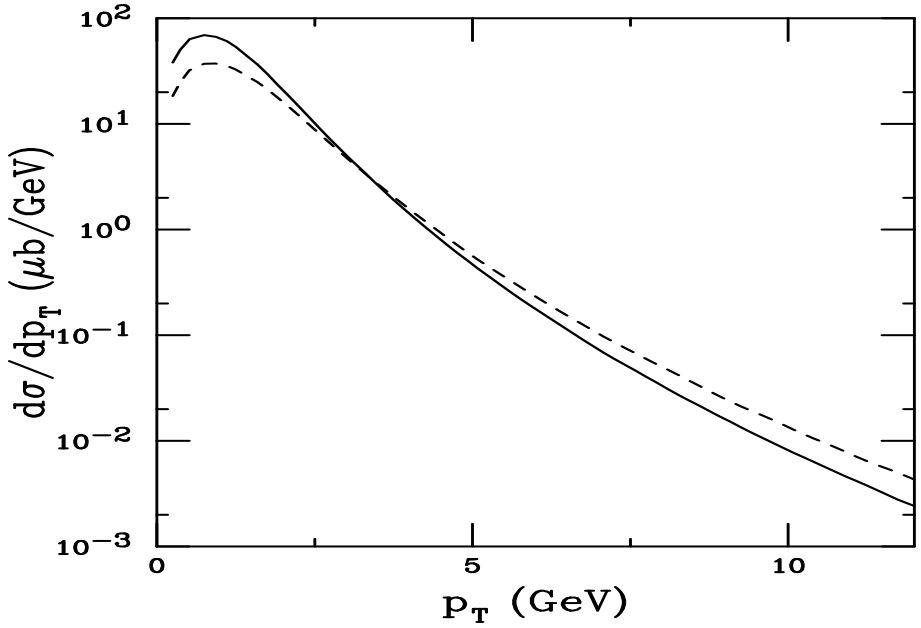

Figure 8: The NLO bare charm quark distributions at $\sqrt{S} = 200$ GeV. The dashed curve shows the NLO calculation with the GRV98 HO parton densities, $m = 1.3$ GeV and $\mu = m_T$ while the solid curve is the result with MRST HO parton densities, $m = 1.2$ GeV and $\mu = 2m_T$.

Comparison With STAR Data

Some of the p_T distributions shown previously compared to STAR data

Good agreement with shape but not normalization (curves scaled up by a factor of four)

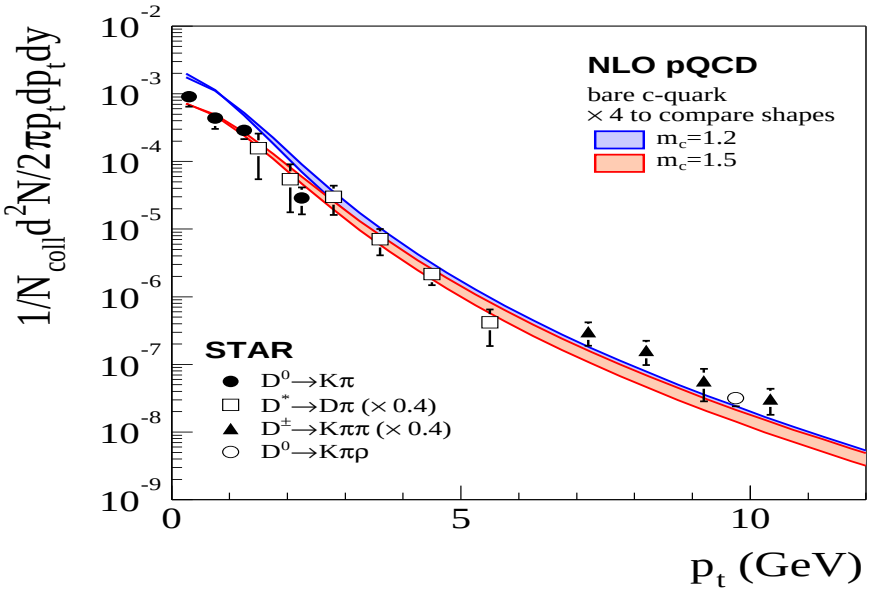

Figure 9: The STAR D meson data is compared to NLO bare charm calculations. The curves, calculated with the GRV98 HO parton densities, show a range of mass and scale values. They are scaled by a factor of 4 to agree with the normalization of the data. [M. van Leeuwen, SQM'04.]

Charm Not at Very Low x at RHIC

Compare μ^2 and x at several values of charm quark rapidity when rapidity of unobserved c (or $\overline{c}$) integrated away, $m = 1.2$ GeV, $\mu^2 = 4m_T^2$

$x_2 = (2m_T/\sqrt{S})(\exp(-y) + \exp(-y_2)) \geq 0.01$ at LO, not symmetric around $y = 0$

Higher energies (and forward rapidities) needed to reach the low x regime

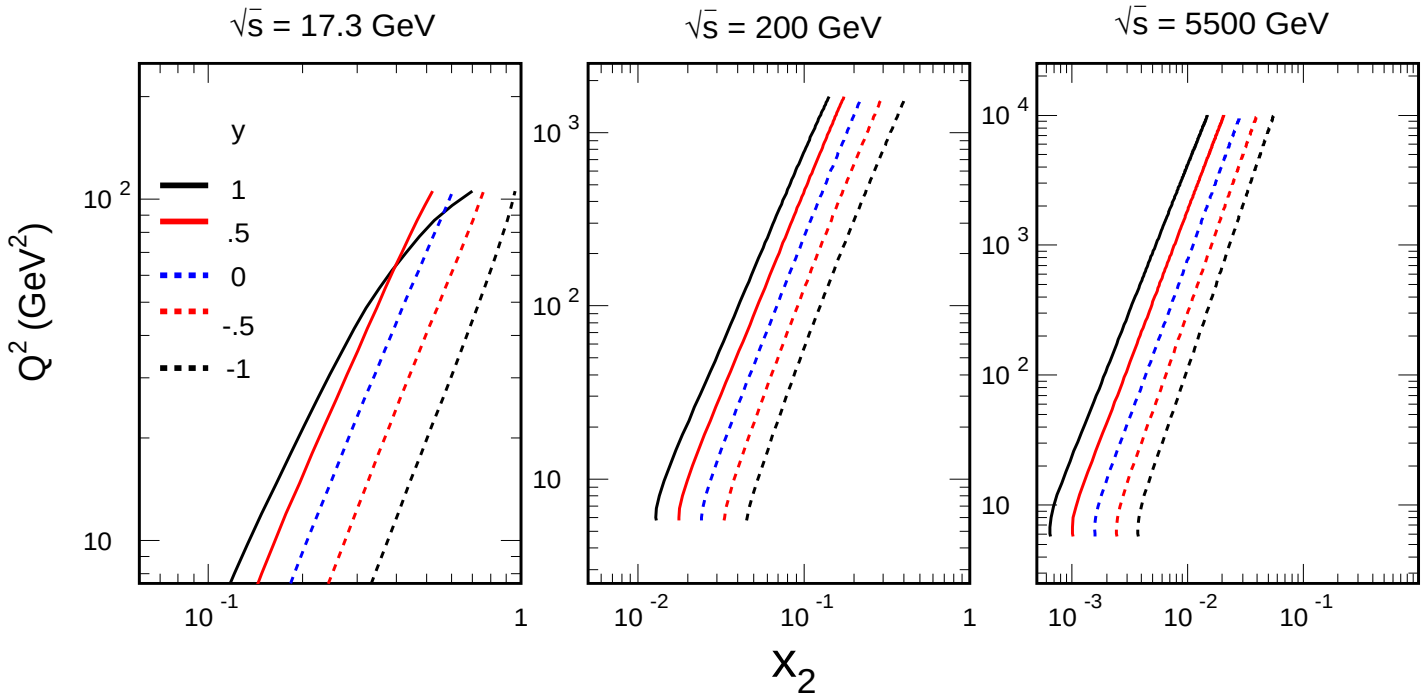

Figure 10: Curves of Q^2 as a function of x_2 for $y = 1$, 0.5, 0, -0.5 and -1 when the rapidity of the unobserved quark is integrated away. (With N. Xu and L. Grandchamp.)

CDF Data Agrees with NLO Bare Charm Distribution

CDF data shown are sum of D^+ and D^0 (and conjugate) distributions, error bars are convolution of statistical and systematic errors

No rescaling is needed to reach agreement with the data

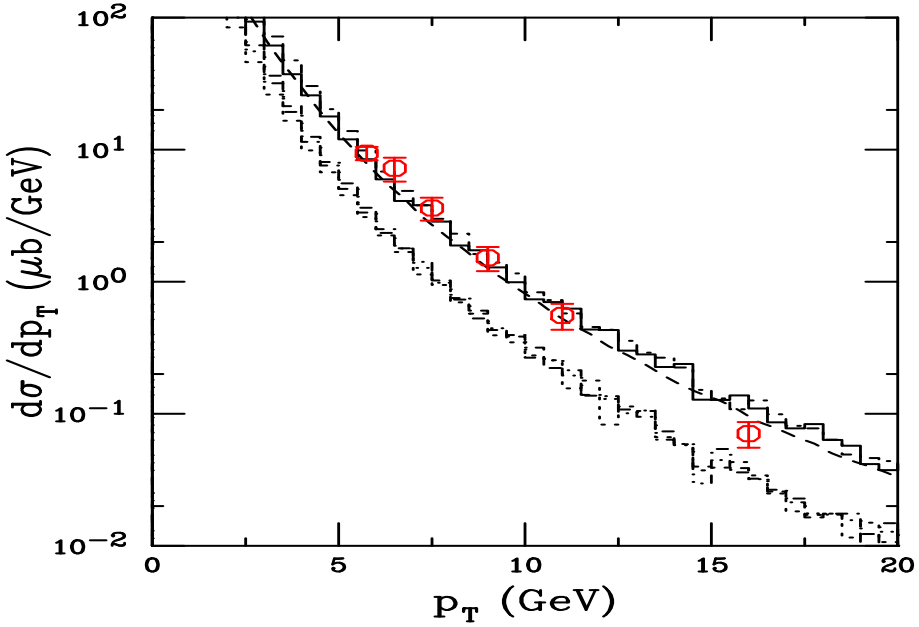

Figure 11: We compare the NLO p_T distributions including fragmentation and intrinsic k_T at $\sqrt{S_{NN}} = 1.96$ TeV compared to the CDF data. The upper solid histogram and curve shows the bare distribution, the dashed includes $\langle k_T^2 \rangle = 1$ GeV^2 but no fragmentation, the dot-dashed is Peterson fragmentation alone, the dotted and lower solid include both Peterson fragmentation and broadening with $\langle k_T^2 \rangle = 1$ and 1.7 GeV^2 respectively.

Why Doesn't Fragmentation Agree With Data?

- Effect of intrinsic k_T weak at high energy where $\langle p_T \rangle$ of heavy quark is larger than at fixed-target energies
- Peterson function is old, assumes charm quark loses on average 30% of its momentum, may be newer parameterizations which reduce momentum loss
- Violation of factorization? Either fragmentation may not be universal or we just don't understand it well enough yet
- What about coalescence? In hadronic hard scatterings, initial hadrons break up, freeing partons comoving with the charm quark to coalesce into hadron with little momentum loss (suggested by R.V., Brodsky and Hoyer, 92)

Influence on J/ψ of Large $\sigma_{c\overline{c}}$

Regeneration of J/ψ possible when more than 1 $c\overline{c}$ pair produced per event

$\sigma_{c\overline{c}} \approx 0.35$ mb from pQCD, about 8 $c\overline{c}$ pairs/event

Preliminary STAR cross section, $1.1 - 1.4$ mb, $26 - 33$ $c\overline{c}$/event, increasing J/ψ yield per collision

Increase inconsistent with PHENIX Au+Au data, PHENIX pp result more consistent with pQCD

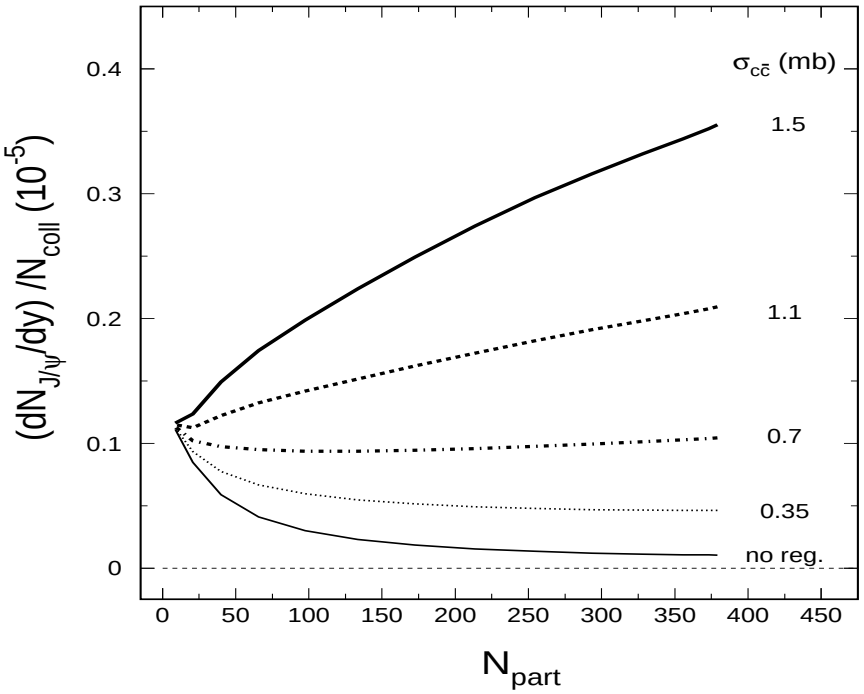

Figure 12: The effect of various values of the $c\overline{c}$ total cross section on the number of J/ψ produced per binary collision as a function of the number of participants. (With N. Xu and L. Grandchamp.)

PHENIX J/ψ pp Rapidity Distribution Like pQCD

No scaling needed to obtain reasonable agreement with data, newer data are lower

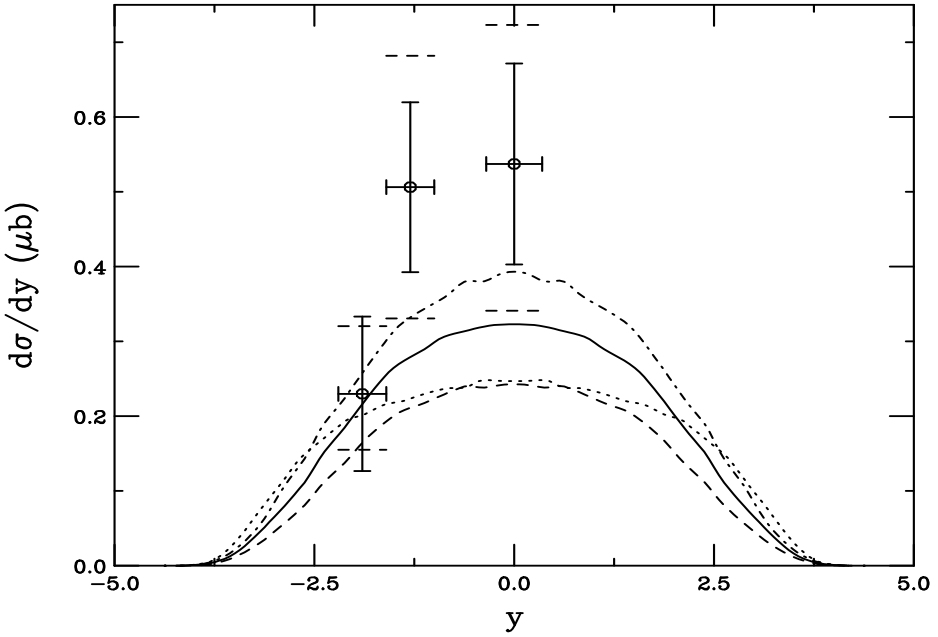

Figure 13: Direct J/ψ rapidity distributions compared to PHENIX data from Quark Matter '02. The data points are scaled to remove the $J/\psi \to l^+l^-$ branching ratio and to include direct production only. The solid curve employs the MRST HO distributions with $m = \mu/2 = 1.2$ GeV, the dashed, MRST HO with $m = \mu = 1.4$ GeV, the dot-dashed, CTEQ 5M with $m = \mu/2 = 1.2$ GeV, and the dotted, GRV 98 HO with $m = \mu = 1.3$ GeV.

Charmonium Production in the Color Evaporation Model (CEM)

Gavai *et al.*, G. Schuler and R.V.

All charmonium states are treated like $c\overline{c}$ below $D\overline{D}$ threshold

Distributions for all charmonium family members identical

At LO, $gg \to c\overline{c}$ and $q\overline{q} \to c\overline{c}$; NLO add $gq \to c\overline{c}q$

$$\sigma_C^{\rm CEM} = F_C \sum_{i,j} \int_{4m^2}^{4m_D^2} d\hat{s} \int dx_1 dx_2 \; f_{i/p}(x_1,\mu^2) \; f_{j/p}(x_2,\mu^2) \; \hat{\sigma}_{ij}(\hat{s}) \; \delta(\hat{s} - x_1 x_2 s)$$

F_C fixed at NLO

Data and branching ratios can be used to separate out the F_C's for each state in quarkonium family

Values of m and μ^2 for several parton densities fixed from $c\overline{c}$ production

Extrapolated J/ψ Total Cross Sections

Total forward J/ψ cross sections extrapolated to higher energy

Energy dependence obtained from NLO CEM

Factor of $\sim 1.6-2$ between results at 200 GeV and at 5.5 TeV

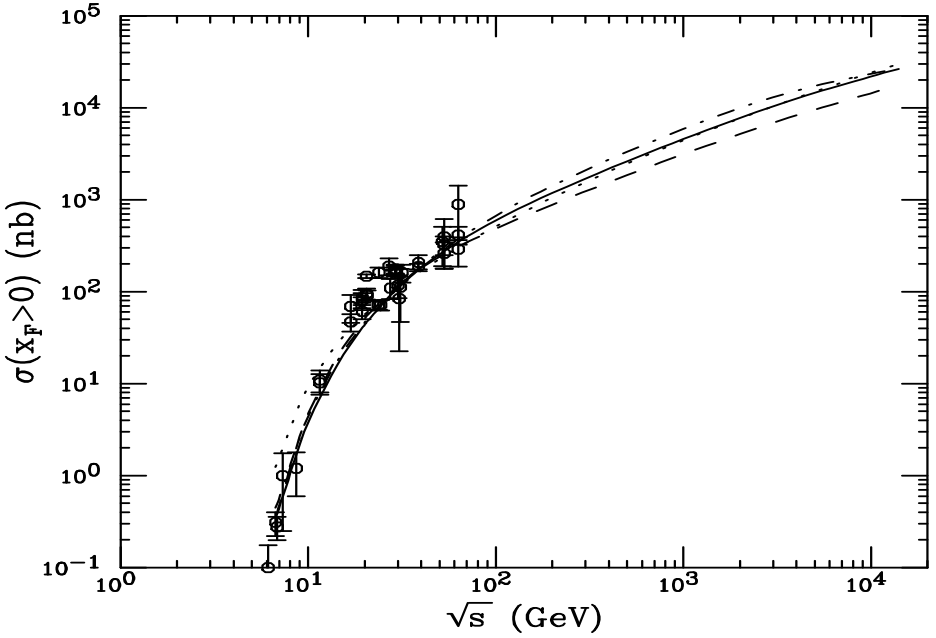

Figure 14: NLO J/ψ forward cross sections. The solid curve employs the MRST HO distributions with $m = \mu/2 = 1.2$ GeV, the dashed, MRST HO with $m = \mu = 1.4$ GeV, the dot-dashed, CTEQ 5M with $m = \mu/2 = 1.2$ GeV, and the dotted, GRV 98 HO with $m = \mu = 1.3$ GeV.

Average x_2 as a Function of Energy and Rapidity

We calculate $\langle x_2 \rangle$ as a function of rapidity in the CEM (N.B. $\langle x_1 \rangle$ is mirror imagine of $\langle x_2 \rangle$)

Increasing $\sqrt{S}$ broadens y range and decreases x_2

In PHENIX muon arms, it is possible to reach lower $\langle x_2 \rangle$ than with leading hadrons at similar rapidities: gg dominates and scale is relatively lower

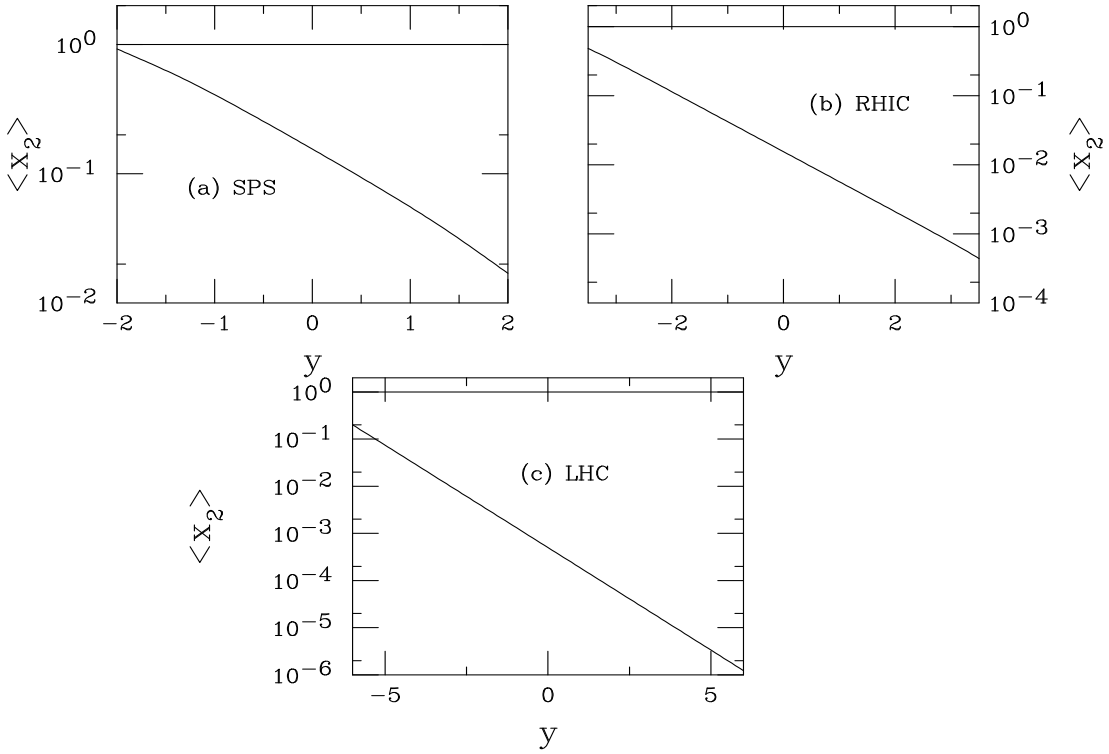

Figure 15: We give the average value of the nucleon momentum fraction, x_2, in pp collisions as a function of rapidity for (a) the CERN SPS with $\sqrt{S} = 19.4$ GeV, (b) RHIC with $\sqrt{S} = 200$ GeV and (c) the LHC with $\sqrt{S} = 6.2$ TeV.

In dA Interactions, Nuclear Effects Should Become Important

Nuclear effects seen to be important in charmonium production at fixed target energies

In extrapolated pA cross sections, the exponent α was shown to be a function of both x_F and p_T

Several mechanisms affect A dependence in cold matter, we consider two here:

- Nuclear Shadowing — initial-state effect on the parton distributions affecting the level of production, important as a function of rapidity/x_F
- Absorption — final-state effect, after $c\overline{c}$ that forms the J/ψ has been produced, pair breaks up in matter due to interactions with nucleons

Nuclear Parton Distributions

Nuclear parton densities

$$F_i^A(x,Q^2,\vec{r},z) = \rho_A(s)S^i(A,x,Q^2,\vec{r},z)f_i^N(x,Q^2)s=\sqrt{b^2+z^2}$$
$$\rho_A(s) = \rho_0\frac{1+\omega(s/R_A)^2}{1+\exp[(s-R_A)/d]}$$

We use EKS98 and Frankfurt, Guzey and Strikman (FGS) parameterizations: original, FGSo, high, FGSh, and low, FGSl, gluon shadowing

EKS98 has no spatial dependence, two FGS inhomogeneous parameterization recently made available — compare our spatial parameterizations with those of FGS

With no nuclear modifications, $S^i(A,x,Q^2,\vec{r},z)\equiv 1$.

Spatial dependence of shadowing

Proportional to local nuclear density:

$$S^i_{\rm WS}=S^i(A,x,Q^2,\vec{r},z) = 1+N_{\rm WS}[S^i(A,x,Q^2)-1]\frac{\rho(s)}{\rho_0}$$

Proportional to nuclear path length:

$$S^i_\rho(A,x,Q^2,\vec{r},z)=1+N_\rho(S^i(A,x,Q^2)-1)\frac{\int dz\rho_A(\vec{r},z)}{\int dz\rho_A(0,z)}\ .$$

Normalization: $(1/A)\int d^2rdz\rho_A(s)S^i_{{\rm WS},\rho}\equiv S^i$. Larger than average modifications for $b=0$. Nucleons like free protons when $s\gg R_A$. Similar normalization for FGS inhomogeneous parameterizations.

Comparing Shadowing Parameterizations: x Dependence

Recent parameterizations by Frankfurt *et al* use EKS98 for valence shadowing, stronger gluon shadowing at low x, cuts off modification above $x = 0.25$ for sea, 0.03 for gluon

Newer FGS parameterizations have lower gluon antishadowing, smoother x dependence over $10^{-4} < x < 0.02$.

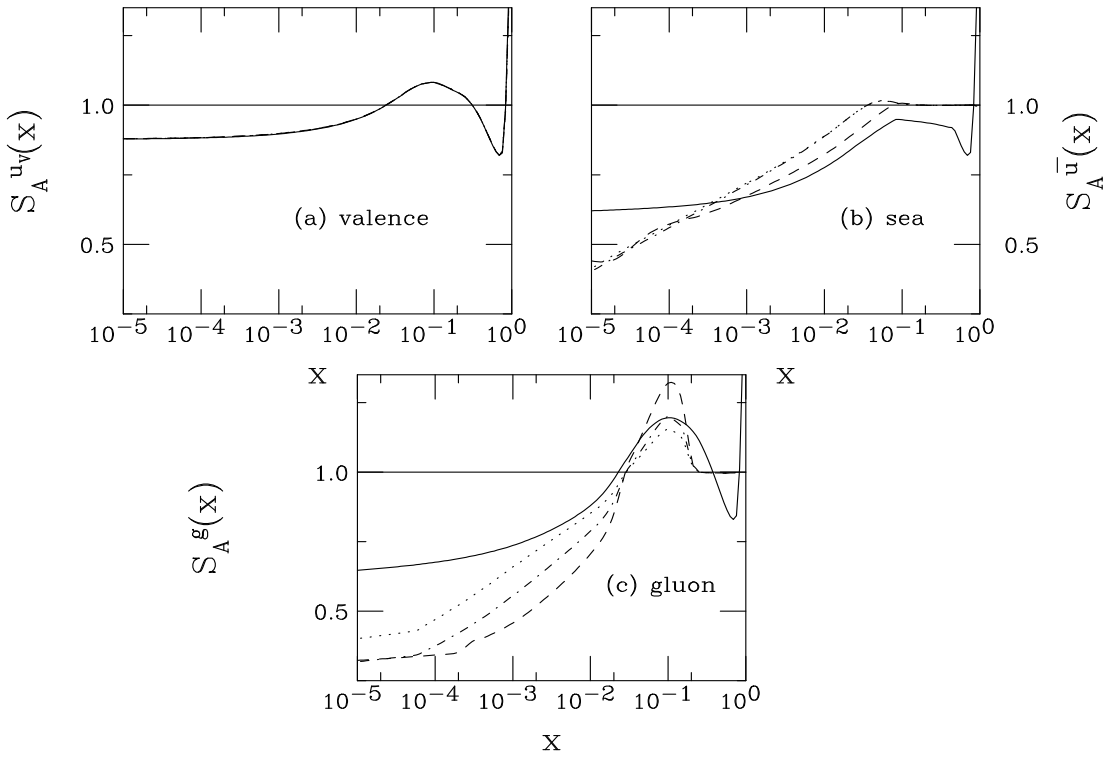

Figure 16: The EKS98 and FGS shadowing parameterizations are compared at the scale $\mu = 2m = 2.4$ GeV. The solid curves are the EKS98 parameterization, the dashed, FGSo, dot-dashed, FGSh, dotted, FGSl.

Comparing Shadowing Parameterizations: b Dependence

Path length, ρ, parameterization is most similar to FGS inhomogeneous parameterizations

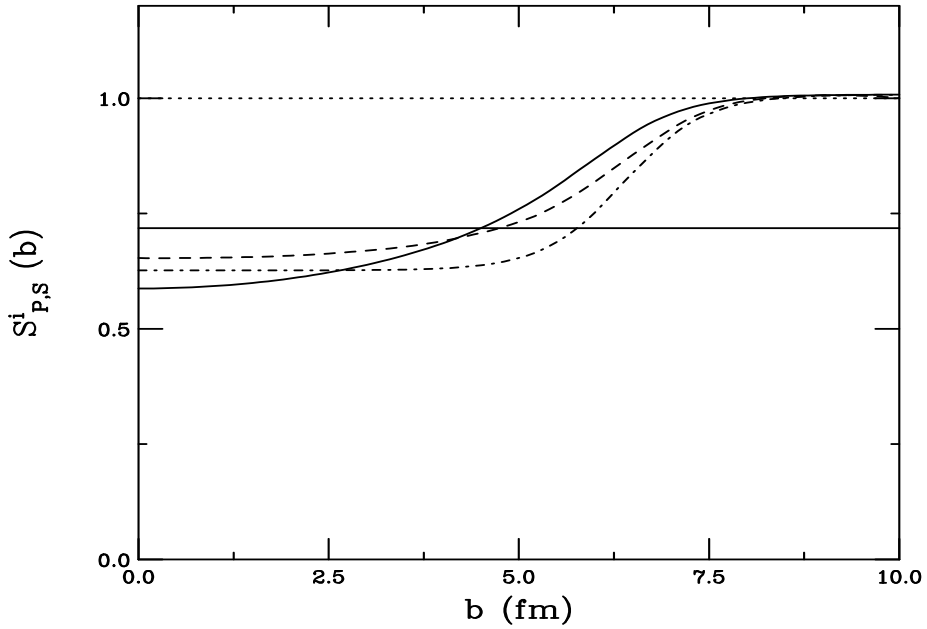

Figure 17: The WS (dot-dashed) and ρ (solid) inhomogeneous shadowing parameterizations are compared to the inhomogeneous FGS shadowing parameterization (dashed) at similar values of homogeneous shadowing, indicated by the solid line.

Effect on J/ψ pAu/pp Ratios

Ratios at LO with MRST LO PDFs and the NLO ratios with MRST HO PDFs give similar results

Frankfurt *et al* parameterization has a bigger effect at large rapidity

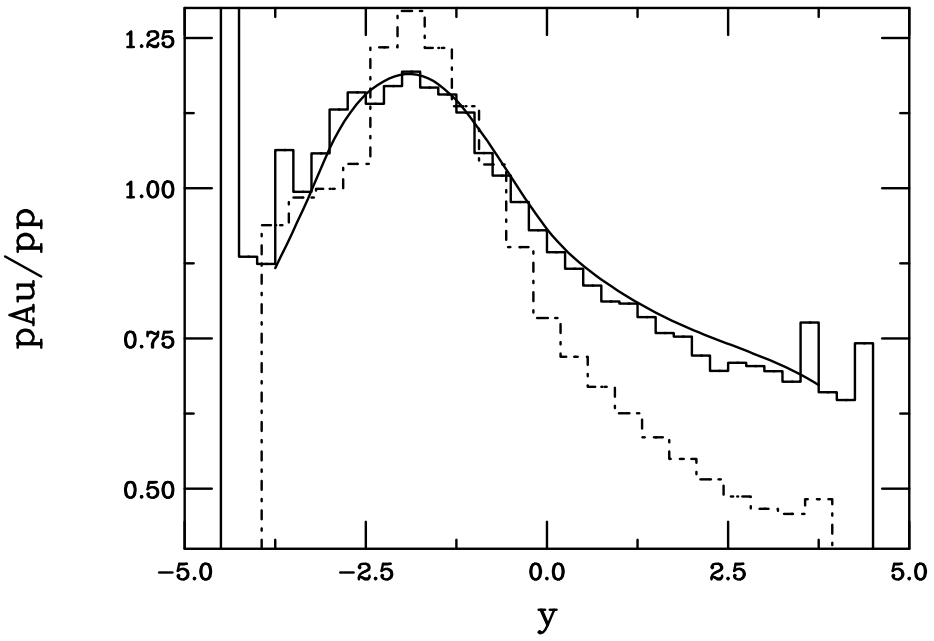

Figure 18: The J/ψ pAu/pp ratio at 200 GeV at NLO (solid histogram, using the MRST HO distributions with $m = \mu/2 = 1.2$ GeV), at LO (solid curve using the MRST LO distributions with the same mass and scale) calculated with the EKS98 parameterization are compared. The ratio with the same parameters and the FGS shadowing parameterization is given in the dashed histogram.

Inohomogeneous Shadowing Effects in y and b

EKS98 and FGSo results show stronger shadowing for central impact parameters, reduced effect in peripheral bins, b-integrated results equivalent to homogeneous shadowing

FGSh and FGSl have stronger b dependence because b range is $0.587 \leq b \leq 10$ fm: shadowing goes away at $b/R_A \sim 1.5$.

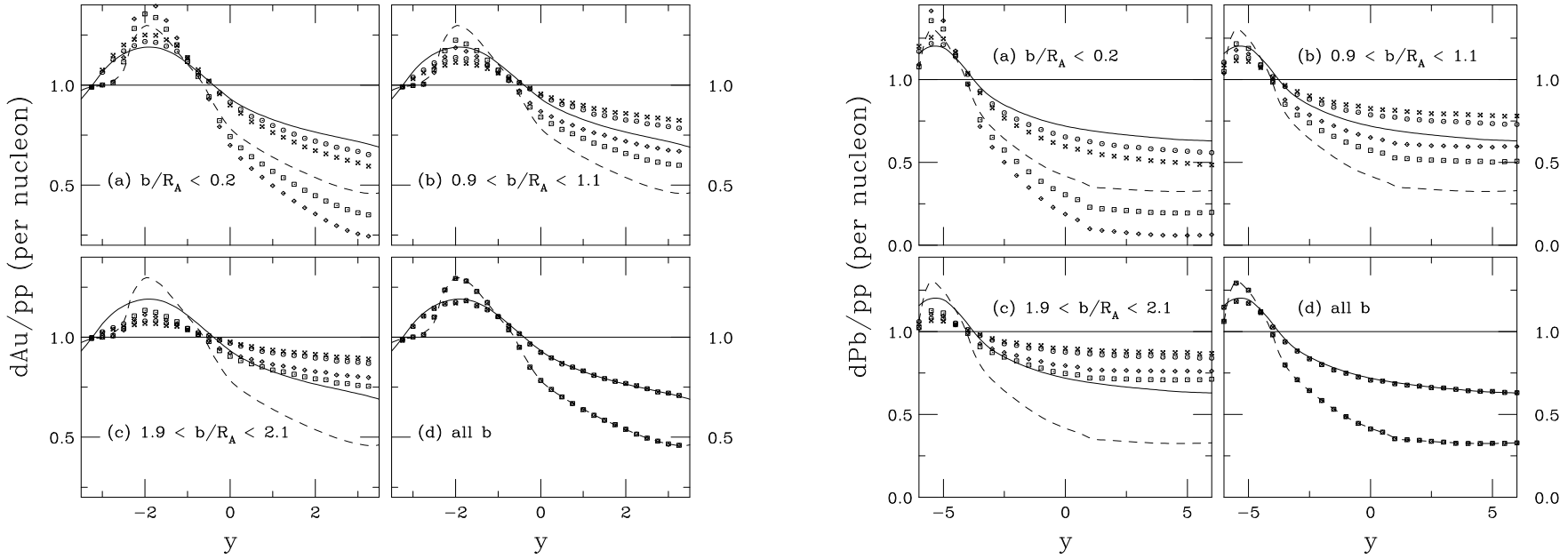

Figure 19: The J/ψ dA/pp ratio at 200 GeV (left) and 6.2 TeV (right) as a function of rapidity. The results are shown for the EKS98 (solid – homogeneous shadowing, circles and x's – inhomogeneous shadowing assuming SEKS, WS and $S_{\mathrm{EKS},\rho}$) and FGSo (dashed – homogeneous shadowing, squares and diamonds – inhomogeneous shadowing assuming $S_{\mathrm{FGSo,\,WS}}$ and $S_{\mathrm{FGSo},\rho}$). The bins are (a) $b/R_A < 0.2$, (b) $0.9 < b/R_A < 1.1$, (c) $1.9 < b/R_A < 2.1$ and (d) all b.

PHENIX J/ψ Data Show Modification of Nuclear PDFs

Little effect at midrapidity but suppression seen at forward η

Nuclear shadowing alone gives fair agreement with data but absorption still needs to be included on a reasonable level .

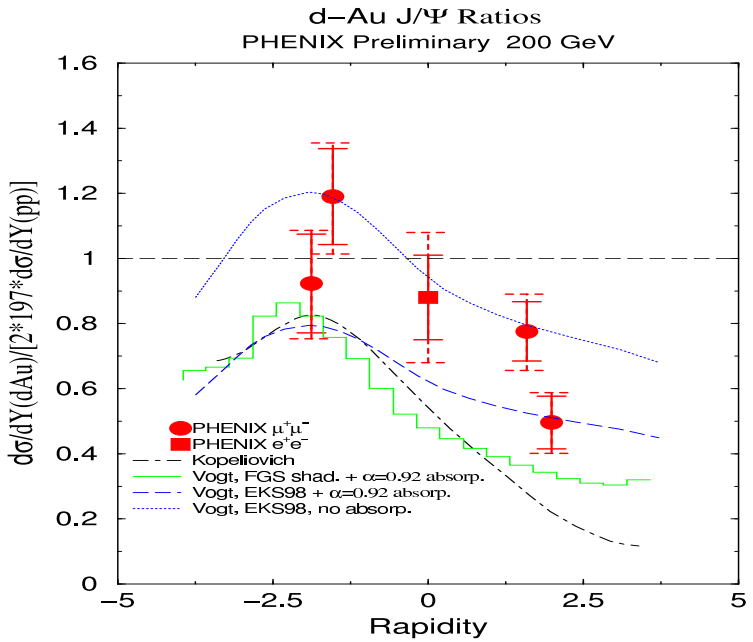

Figure 20: PHENIX d+Au/pp ratio for J/ψ production as a function of rapidity. The curves are theory calculations. The upper curve is EKS98 shadowing with no absorption. The lower shadowing curves have nuclear absorption added in by scaling the shadowing curves by A^α with $\alpha = 0.92$. [From PHENIX Collaboration, QM'04 proceedings.]

J/ψ Absorption by Nucleons

Woods-Saxon nuclear density profiles typically used

$$\begin{aligned}\sigma_{pA} &= \sigma_{pN}\int d^2b \int_{-\infty}^{\infty} dz\, \rho_A(b,z) S_A^{\rm abs}(b) \\ &= \sigma_{pN}\int d^2b \int_{-\infty}^{\infty} dz\, \rho_A(b,z) \exp\left\{-\int_z^{\infty} dz' \rho_A(b,z')\sigma_{\rm abs}(z'-z)\right\}\end{aligned}$$

Note that if $\rho_A = \rho_0$, $\alpha = 1 - 9\sigma_{\rm abs}/(16\pi r_0^2)$

We discuss absorption of color singlet and color octet states in the CEM and a combination of the two in NRQCD

Singlet Absorption Model

All $c\overline{c}$ pairs assumed to be produced in small color singlet states

Assume quadratic growth of cross section with proper time until formation time τ_F (Blaizot and Ollitrault)

Strongest at low to negative x_F where J/ψ can form in the target

Asymptotic ψ' and χ_c cross sections proportional to the final state meson size, *e.g.* $\sigma^{\rm s}_{\psi' N} = \sigma^{\rm s}_{J/\psi N}(r_{\psi'}/r_{J/\psi})^2$ (Povh and Hüfner)

$$\sigma_{\rm abs}(z'-z) = \begin{cases} \sigma^{\rm s}_{CN}(\dfrac{\tau}{\tau_F^C})^2 & \text{if } \tau < \tau_F^C \\ \sigma^{\rm s}_{CN} & \text{otherwise} \end{cases} .$$

$$\begin{aligned} \tau_F^{J/\psi} &= 0.92 \text{ fm} \qquad & \sigma^{\rm s}_{J/\psi N} &\sim 2.5 \text{ mb} \\ \tau_F^{\psi'} &= 1.5 \text{ fm} \qquad & \sigma^{\rm s}_{\psi' N} &= 3.7\,\sigma^{\rm s}_{J/\psi N} \\ \tau_F^{\chi_c} &= 2 \text{ fm} \qquad & \sigma^{\rm s}_{\chi_c N} &= 2.4\,\sigma^{\rm s}_{J/\psi N} \end{aligned}$$

Octet Absorption Model

Pre-resonant $c\overline{c}$ pairs travel through the nucleus as $|(c\overline{c})_8 g\rangle$ color octet states

Characteristic octet lifetime $\tau_8 \sim 0.25$ fm

For $x_F \geq -0.1$, path length of $|(c\overline{c})_8 g\rangle$ through the target from its production point is greater than maximum path length

These fast states pass through nucleus in color octets so that the pre-resonant A dependence is the same for J/ψ, ψ' and χ_c (Kharzeev and Satz) — $\sigma^{\rm o}_{\rm abs} = 3$ mb agrees with E866 forward A dependence

Universal constant absorption cross section usually assumed for nuclear collision studies (NA38, NA50) where $0 < x_F < 0.18$

At negative x_F, path length is shorter and octet state can neutralize its color inside target and be absorbed as color singlet

Only J/ψ likely to be fully formed inside target even though color neutralization may occur for all states

We compare results with no octet to singlet conversion (constant octet) and with conversion (growing octet)

Singlet + Octet Absorption

Relative contributions of singlet and octet production set by NRQCD (Zhang *et al.*)

Equal absorption cross sections for all octet states

Singlet cross sections set by final state size

$$\frac{d\sigma_{pA}^{\psi}}{dx_F} = \int d^2b \left[\frac{d\sigma_{pp}^{\psi,\,\mathrm{oct}}}{dx_F} T_A^{\psi,\mathrm{eff\ (oct)}}(b) + \frac{d\sigma_{pp}^{\psi,\,\mathrm{sing}}}{dx_F} T_A^{\psi,\mathrm{eff\ (sing)}}(b) \right] ,$$

$$\frac{d\sigma_{pA}^{\chi_{cJ}\to J/\psi X}}{dx_F} = \int d^2b \sum_{J=0}^{2} B(\chi_{cJ} \to J/\psi X) \left[\frac{d\sigma_{pp}^{\chi_{cJ},\,\mathrm{oct}}}{dx_F} T_A^{\chi_{cJ},\mathrm{eff\ (oct)}}(b) + \frac{d\sigma_{pp}^{\chi_{cJ},\,\mathrm{sing}}}{dx_F} T_A^{\chi_{cJ},\mathrm{eff\ (sing)}}(b) \right] ,$$

$$\begin{aligned}
\frac{d\sigma_{pA}^{J/\psi,\,\mathrm{tot}}}{dx_F} = \int d^2b \Bigg\{ & \Bigg[\frac{d\sigma_{pp}^{J/\psi,\,\mathrm{dir,\,oct}}}{dx_F} T_A^{J/\psi,\mathrm{eff\ (oct)}}(b) \\
& + \sum_{J=0}^{2} B(\chi_{cJ} \to J/\psi X) \frac{d\sigma_{pp}^{\chi_{cJ},\,\mathrm{oct}}}{dx_F} T_A^{\chi_{cJ},\mathrm{eff\ (oct)}}(b) + B(\psi' \to \psi X) \frac{d\sigma_{pp}^{\psi',\,\mathrm{oct}}}{dx_F} T_A^{\chi_{cJ},\mathrm{eff\ (oct)}}(b) \Bigg] \\
& + \Bigg[\frac{d\sigma_{pp}^{J/\psi,\,\mathrm{dir,\,sing}}}{dx_F} T_A^{J/\psi,\mathrm{dir,eff\ (sing)}}(b) + \sum_{J=0}^{2} B(\chi_{cJ} \to \psi X) \frac{d\sigma_{pp}^{\chi_{cJ},\,\mathrm{sing}}}{dx_F} T_A^{\chi_{cJ},\,\mathrm{eff\ (sing)}}(b) \\
& + B(\psi' \to \psi X) \frac{d\sigma_{pp}^{\psi',\,\mathrm{sing}}}{dx_F} T_A^{\psi',\,\mathrm{eff\ (sing)}}(b) \Bigg] \Bigg\}
\end{aligned}$$

$$T_A^{\mathrm{eff}}(b) = \int_{-\infty}^{\infty} dz\, \rho_A(b,z) \exp\left\{ - \int_z^{\infty} dz' \rho_A(b,z') \sigma_{\mathrm{abs}}(z'-z) \right\}$$

Rapidity dependence of Homogeneous Absorption

Results shown for different charmonium states: inclusive and direct J/ψ, ψ' and χ_c

Constant and growing octet indistinguishable in detector range, singlet absorption only effective for $y < -1$ (RHIC) and $y < -5$ (LHC), NRQCD also shows little rapidity dependence

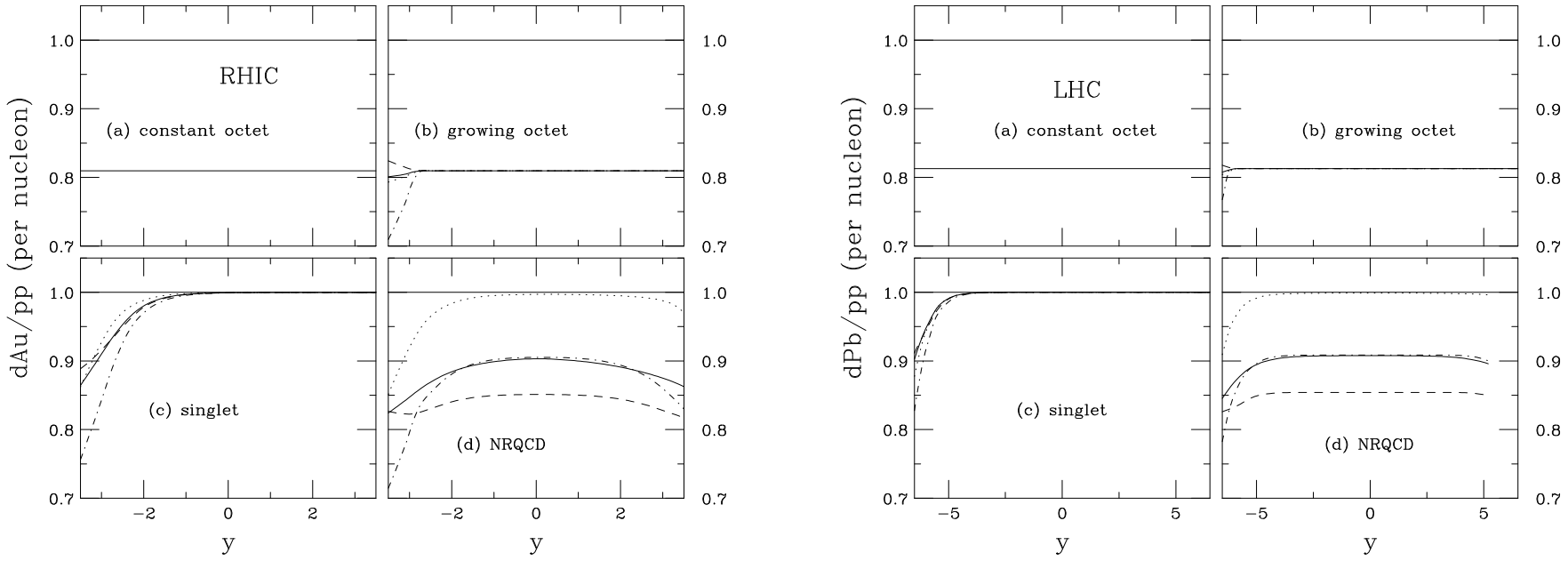

Figure 21: The J/ψ dAu/pp ratio at 200 GeV (left) and 6.2 TeV (right) as a function of rapidity for absorption alone. We show (a) constant octet with 3 mb, (b) growing octet with 3 mb asymptotic cross section for all states, (c) singlet with 2.5 mb J/ψ absorption cross section, all calculated in the CEM and (d) NRQCD with a combination of octet and singlet matrix elements. The curves show total J/ψ (solid), direct J/ψ (dashed), ψ' (dot-dashed) and χ_c (dotted).

Effect of Inhomogeneous Absorption

Example of impact parameter dependence of absorption

Solid curve is 3 mb constant octet cross section, all rapidities, dashed is at $y = -2$, singlet

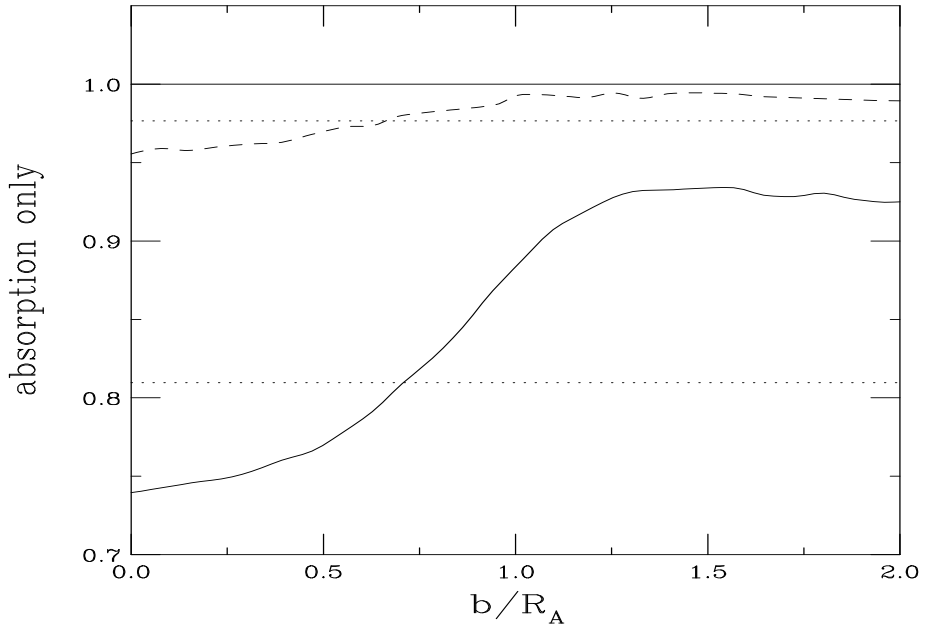

Figure 22: The J/ψ dAu/pp ratio as a function of b for absorption alone with $\sigma_{\rm abs} = 3$ mb for a constant octet (all y), solid, and singlet ($y = -2$), dashed. The homogeneous results are indicated by the dotted lines.

Homogeneous Absorption and Shadowing at RHIC

Left-hand side: Effect of $\sigma_{\rm abs}$ is shown for various absorption models

Right-hand side: Comparing shadowing parameterizations for $\sigma_{\rm abs} = 3$ mb, FGSl similar to EKS98

.

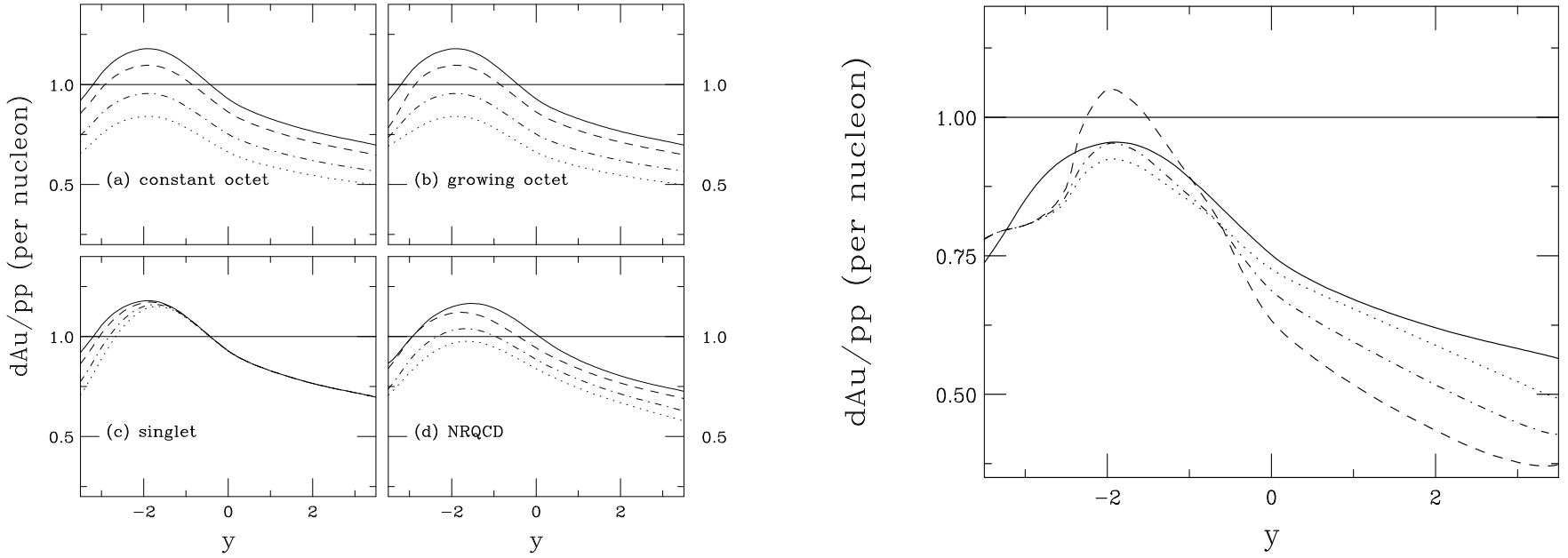

Figure 23: Left-hand side: The J/ψ dAu/pp ratio at 200 GeV with the EKS98 shadowing parameterization as a function of rapidity for our absorption models: (a) constant octet, (b) growing octet, (c) singlet and (d) a combination of octet and singlet. In (a)-(c), the curves are no absorption (solid), $\sigma_{\rm abs} = 1$ (dashed), 3 (dot-dashed) and 5 mb (dotted). In (d), the results are no absorption (solid), 1 mb octet/1 mb singlet (dashed), 3 mb octet/3 mb singlet (dot-dashed), and 5 mb octet/3 mb singlet (dotted). Right-hand side: Comparison of the results for a 3 mb growing octet absorption cross section with the EKS98 (solid), FGSo (dashed), FGSh (dot-dashed) and FGSl (dotted) shadowing parameterizations.

Homogeneous Absorption and Shadowing at the LHC

Left-hand side: J/ψ only produced inside nucleus for $y < -5$, no difference between octet results

Right-hand side: Potentially very large J/ψ suppression at $y > -2$, particularly for FGSo

All FGS parameterizations have stronger shadowing than EKS98 for $y > 0$

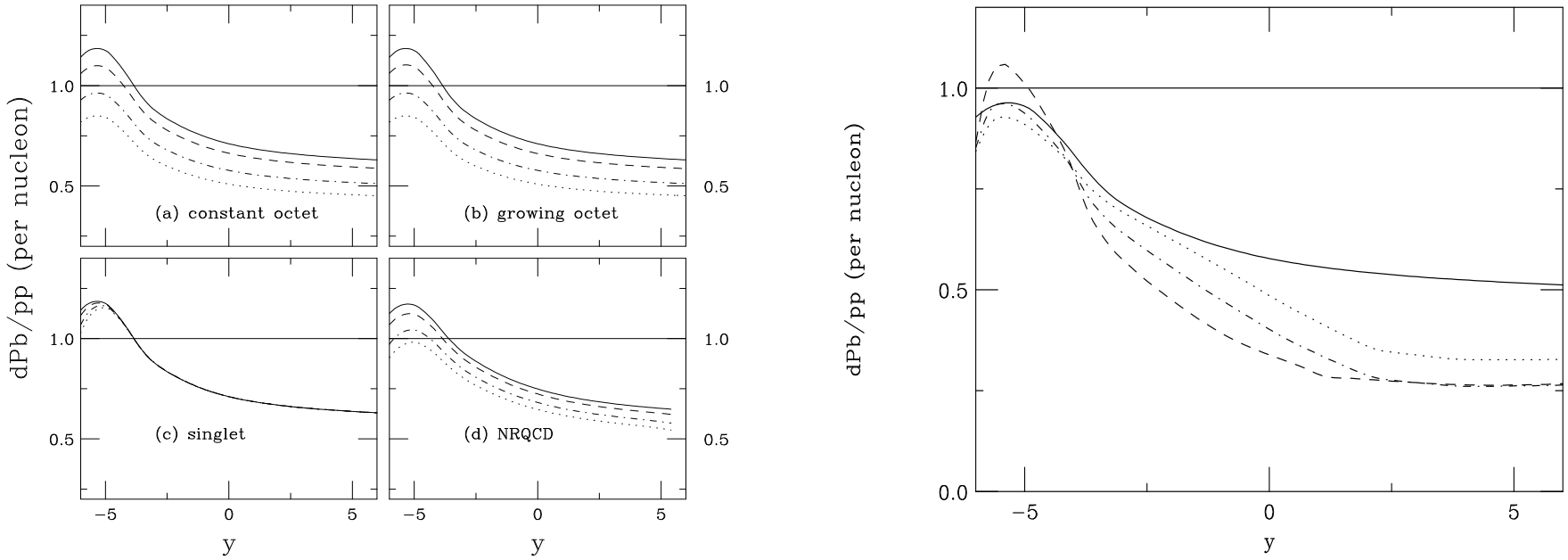

Figure 24: Left-hand side: The J/ψ dPb/pp ratio at 6.2 TeV with the EKS98 shadowing parameterization as a function of rapidity for our absorption models: (a) constant octet, (b) growing octet, (c) singlet and (d) a combination of octet and singlet. In (a)-(c), the curves are no absorption (solid), $\sigma_{\rm abs} = 1$ (dashed), 3 (dot-dashed) and 5 mb (dotted). In (d), the results are no absorption (solid), 1 mb octet/1 mb singlet (dashed), 3 mb octet/3 mb singlet (dot-dashed), and 5 mb octet/3 mb singlet (dotted). Right-hand side: Comparison of the results for a 3 mb growing octet absorption cross section with the EKS98 (solid), FGSo (dashed), FGSh (dot-dashed) and FGSl (dotted) shadowing parameterizations.

Inhomogeneous Shadowing and Absorption at RHIC

PHENIX results presented as a function of $N_{\rm coll}$, the convolution of the nuclear profile functions multiplied by the inelastic NN cross section, 42 mb at RHIC

$$N_{\rm coll}(b) = \sigma_{NN}^{\rm in} \int d^2s T_A(s) T_B(|\vec{b} - \vec{s}|)$$

Results with EKS98 compared at $y = -2$ (antishadowing), 0 (transition region) 2 (shadowing)

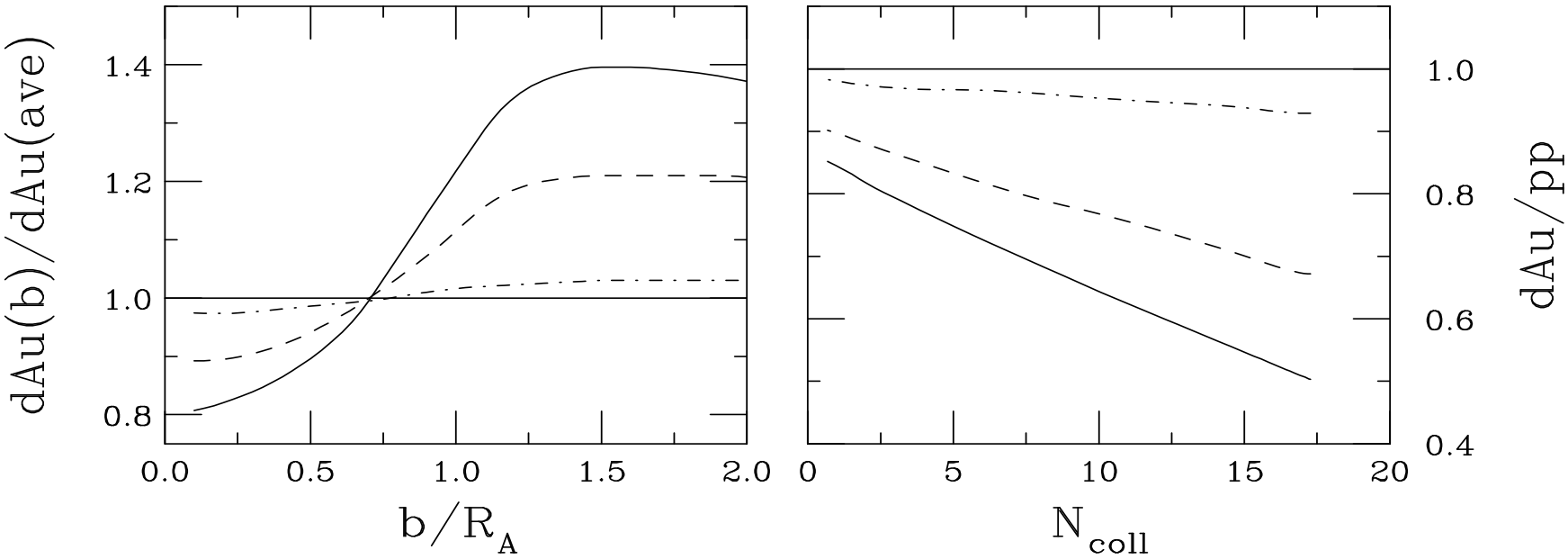

Figure 25: Left-hand side: The J/ψ ratio (dAu(b)/pp)/(dAu(ave)/pp) as a function of b/R_A. Right-hand side: The ratio dAu/pp as a function of $N_{\rm coll}$. Results are shown for $y = -2$ (dot-dashed), $y = 0$ (dashed) and $y = 2$ (solid) at 200 GeV for a growing octet with $\sigma_{\rm abs} = 3$ mb and the EKS98 parameterization.

Comparison of $N_{\rm coll}$ Dependence at RHIC

Path length parameterization,$S_{{\rm P},\rho}$, with EKS98 and FGSo gives linear $N_{\rm coll}$ dependence due to long tails of density distributions

FGSh and FGSl forced to $S = 1$ at $b = 10$ fm so that as $N_{\rm coll} \to 1$, shadowing disappears and only residual absorption remains

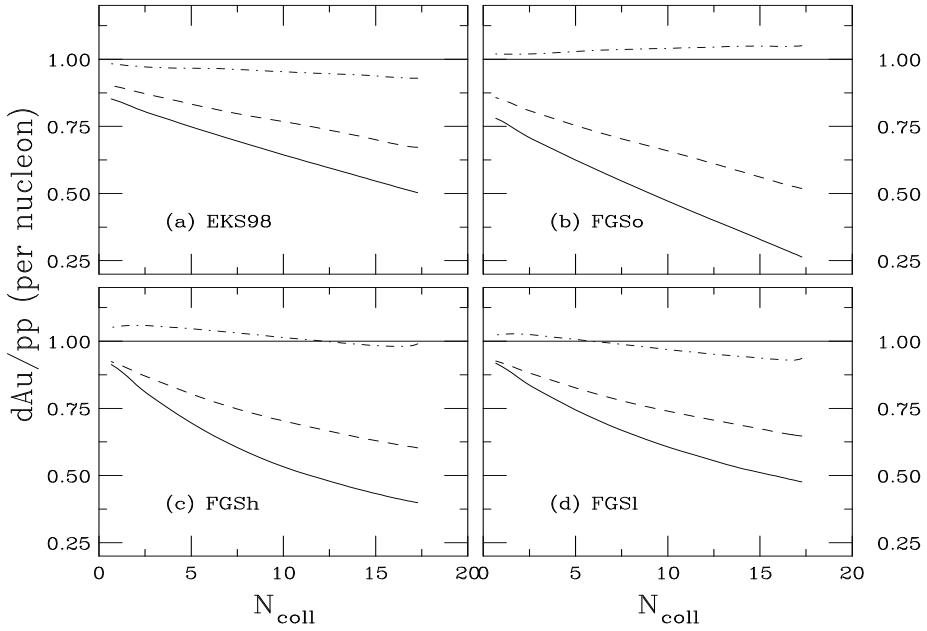

Figure 26: The ratio dAu/pp as a function of $N_{\rm coll}$ for the EKS98 (a), FGSo (b), FGSh (c) and FGSl (d) shadowing parameterizations. The calculations with EKS98 and FGSo use the inhomogeneous path length parameterization while that obtained by FGS is used with FGSh and FGSl. Results are given for $y = -2$ (dot-dashed), $y = 0$ (dashed) and $y = 2$ (solid) at 200 GeV for a growing octet with $\sigma_{\rm abs} = 3$ mb.

Inhomogeneous Shadowing and Absorption at the LHC

LHC results presented as a function of $N_{\rm coll}$ for several rapidities: $y = -4$, -2, 0, 2 and 4, $y = -4$ in $\sim$ antishadowing region

$N_{\rm coll}$ higher here since $\sigma_{NN}^{\rm in} = 76$ mb

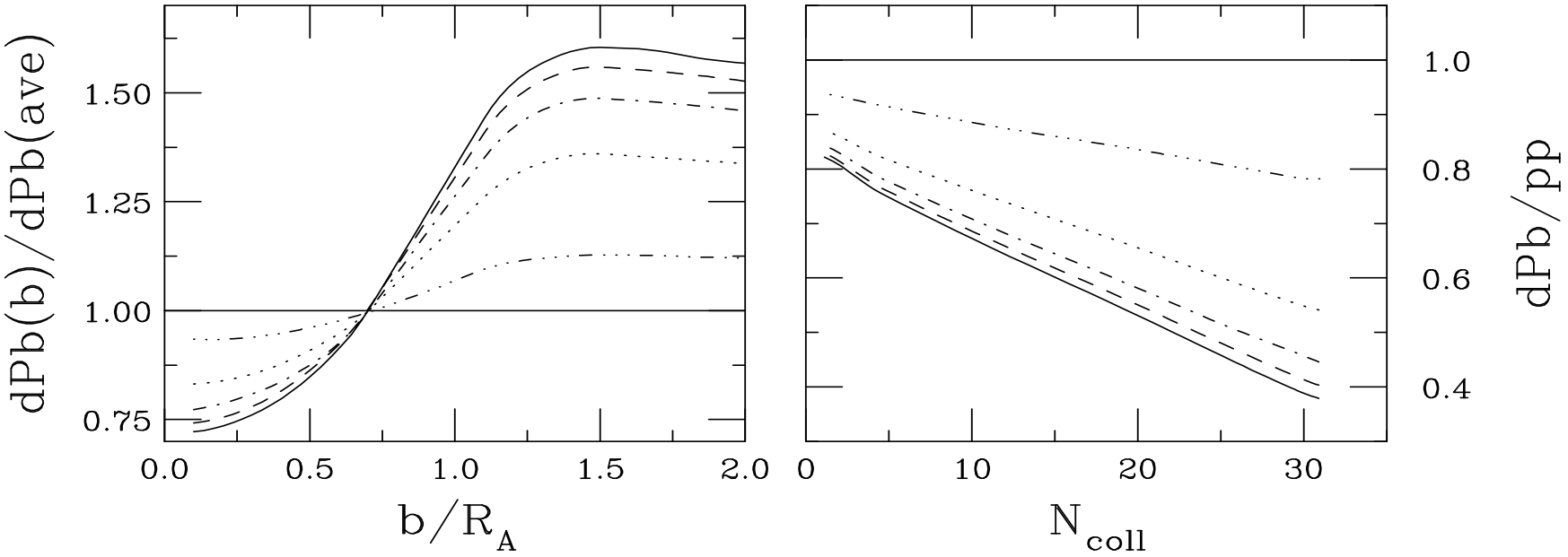

Figure 27: Left-hand side: The J/ψ (dPb(b)/pp)/(dPb(ave)/pp) ratio as a function of b/R_A. Right-hand side: The ratio dPb/pp as a function of $N_{\rm coll}$. Results are shown for $y = -4$ (dot-dot-dot-dashed), $y = -2$ (dotted), $y = 0$ (dot-dashed), $y = 2$ (dashed) and $y = 4$ (solid) at 6.2 TeV for a growing octet with $\sigma_{\rm abs} = 3$ mb and the EKS98 parameterization.

Comparison of $N_{\rm coll}$ Dependence at LHC

Stronger $N_{\rm coll}$ dependence at LHC for FGSh and FGSl due to higher $\sigma_{NN}^{\rm in}$

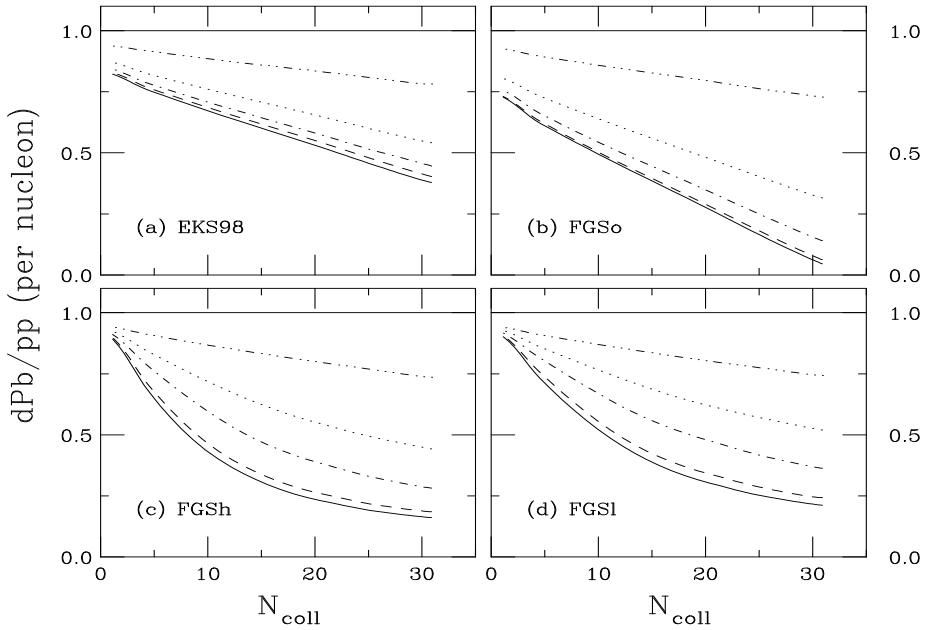

Figure 28: The ratio dPb/pp as a function of $N_{\rm coll}$ for the EKS98 (a), FGSo (b), FGSh (c) and FGSl (d) shadowing parameterizations. The calculations with EKS98 and FGSo use the inhomogeneous path length parameterization while that obtained by FGS is used with FGSh and FGSl. Results are given for $y = -4$ (dot-dot-dot-dashed), $y = -2$ (dotted), $y = 0$ (dot-dashed), $y = 2$ (dashed) and $y = 4$ (solid) at 6.2 TeV for a growing octet with $\sigma_{\rm abs} = 3$ mb.

Summary

Lots of things we don't understand yet

Why is the STAR $c\bar{c}$ cross section so big relative to other recent measurements?

Does fragmentation really factorize?

What is the relative importance of shadowing and absorption in J/ψ production?

How important is regeneration of J/ψ in AA?

How well can we extrapolate to higher energies?

More data will help complete this picture